Title

Using Buckling-Restrained Braces on Long-Span Bridges. I: Full-Scale Testing and Design Implications

Journal

Journal of Bridge Engineering, 21(5)

ISSN

1084-0702

Authors

Lanning, Joel

Benzoni, Gianmario

Uang, Chia-Ming

Publication Date

2016-05-01

DOI

10.1061/(asce)be.1943-5592.0000781

Using Buckling-Restrained Braces on Long-Span Bridges. I: Full-Scale Testing and Design Implications

Joel Lanning, P.E., M.ASCE[1]; Gianmario Benzoni[2]; and Chia-Ming Uang, M.ASCE[3]

Abstract: Using the Vincent Thomas Bridge (VTB) as a feasibility case study, near-fault loading protocols for qualifying buckling-restrained braces (BRBs) for use on long-span bridges were developed and are presented in a companion paper. In this paper, full-scale component testing demonstrated the ability of BRBs to sustain several consecutive near-fault loading protocols, and therefore, they are recommended as qualified for potential use on the VTB and other similar long-span bridges near seismic faults. Near-fault protocol test results led to the proposal of a new procedure for measuring unbalanced BRB compression and tension forces by testing two nominally identical braces. Other novel test variables included the use of stainless steel (SS) for several BRB yielding cores and high strain rates, characteristic of near-fault loading, in two dynamic tests. Design considerations were identified for BRBs using highly ductile SS considering its significant strain-hardening properties, as well as the increased brace force response due to the high strain rate observed for both steels. **DOI: 10.1061/(ASCE)BE.1943-5592.0000781.**

Author keywords: Buckling-restrained braces; Full-scale testing; Near fault; Strain rate; Dynamic testing; Long-span bridges; Stainless steel.

Introduction

Buildings and bridges commonly utilize steel diagonal bracing to provide lateral strength and stiffness. In the seismic design of buildings, some braces are intended to yield in tension and are designed and detailed to inelastically buckle out of plane in compression, serving as a structural fuse protecting vital elements and dissipating energy through material damage. In building frames, these are called special concentrically braced frames (AISC 2010). However, these braces are vulnerable to low-cycle fatigue failure due to highly concentrated deformation in the plastic hinge formed at midlength during inelastic buckling (Bruneau et al. 2011). Therefore, braces capable of yielding in compression without buckling, or buckling-restrained braces (BRBs), have recently become popular in buildings as buckling-restrained braced frames (BRBFs). Although pioneered in the 1970s in Japan, BRBs received little attention until after the 1994 Northridge and 1995 Kobe earthquakes. Afterward, the excellent energy dissipation capabilities of BRBs were widely used in Japan. Once codified in AISC 341-05 for building applications (AISC 2005), BRBFs also quickly became popular in the United States as a ductile seismic force–resisting system (Uang et al. 2004).

BRBs are relatively simple in fabrication and require essentially no maintenance. They primarily consist of a yielding steel core surrounded by, and decoupled from, concrete mortar within a hollow structural section, as shown in Fig. 1(a), along with a schematic representation of the typical stable hysteretic response. As the yielding core of a BRB experiences multiple inelastic excursions, the material undergoes strain hardening, causing brace forces well beyond the initial yield force. Furthermore, during compression excursions, contact friction between the core and the restraining assembly results from both Poisson expansion and restrained inelastic high-mode buckling of the yielding core. Consequently, compression forces are somewhat larger than tension forces at equal and opposite deformations. Hence, a crucial aspect of AISC BRB qualification testing is the determination of the compression strength adjustment factor (β) shown in Fig. 1(b), along with the tension strength adjustment factor (ω). The value of β is limited to 1.3 in AISC 341-10 (AISC 2010), as measured within the AISC protocol, in an attempt to regulate the unbalanced brace forces, making BRBs more amenable to capacity-based design of the adjoining structural members.

BRBs have almost exclusively been used for building applications but have been considered in a few bridge-related research projects and seismic retrofits. Usami et al. (2005) and Kanaji et al. (2005) summarized retrofits of the Owatari and Minato Bridges, respectively, in Japan. Both replaced conventional steel truss members with BRBs to provide ductile truss elements. In the United States, Carden et al. (2004) performed tests using short BRBs in ductile end cross frames for steel plate girders. Pollino and Bruneau (2007) investigated rocking bridge piers with BRBs as passive energy dissipation devices. One known U.S. bridge retrofitted using BRBs is the Auburn-Foresthill Bridge in Auburn, California, which was recently completed and is documented by Reno and Pohll (2010). The BRBs were used to limit the forces imparted to the superstructure, while providing longitudinal stability of the bridge, after yielding of a linkage plate during a large event.

There are currently no established bridge-specific BRB design guidelines or testing requirements. Just as in the early stages of building BRB applications (Uang et al. 2004), thus far, only project-specific requirements and testing programs have been conducted to demonstrate satisfactory performance of proposed BRBs for bridges. This research extends beyond this practice by utilizing a

[1]Assistant Professor, Dept. of Civil and Environmental Engineering, California State Univ., Fullerton, CA 92834 (corresponding author). E-mail: joellanning@fullerton.edu

[2]Research Scientist, Dept. of Structural Engineering, Univ. of California, San Diego, La Jolla, CA 92093. E-mail: gbenzoni@ucsd.edu

[3]Professor, Dept. of Structural Engineering, Univ. of California, San Diego, La Jolla, CA 92093. E-mail: cmu@ucsd.edu

Note. This manuscript was submitted on July 10, 2014; approved on January 26, 2015; published online on January 20, 2016. Discussion period open until June 20, 2016; separate discussions must be submitted for individual papers. This paper is part of the ***Journal of Bridge Engineering***, © ASCE, ISSN 1084-0702.

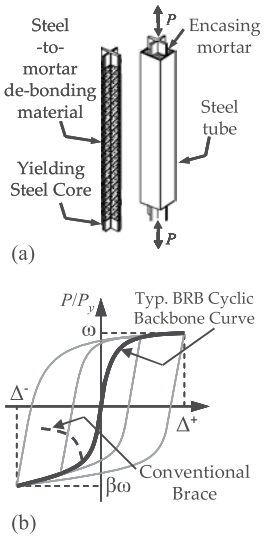

Fig. 1. (a) Basic BRB anatomy; (b) schematic BRB hysteretic response

statistically developed loading protocol for long-span near-fault bridge application of BRBs.

As summarized in the companion paper (Lanning et al. 2015), the authors used the Vincent Thomas Bridge as a case study in which a parametric analysis, using a finite-element model of the bridge, identified BRBs that can fea-sibly replace existing viscous dampers on the bridge for seismic response mitigation; leaking of these viscous dampers has motivated an investigation of a replacement strategy (Benzoni et al. 2008). This long-span suspension bridge is situated directly over the Palos Verdes Fault, making the pre-established site-specific design earthquake a near-fault pulse-type ground motion (Moffatt and Nichol Engineers 1996); these circumstances are common for many long-span bridges in California. Therefore, this scenario presents an important new structural application and seismic environment for BRBs. These earthquakes are characterized by a pulse of high ground velocity that causes the inelastic cyclic demands to be large amplitude, asymmetric, and applied at a high rate, all of which are explicitly neglected in the only existing BRB provisions, AISC 341-10. The loading protocol for brace prequalification given by these provisions (AISC protocol) is based on the effects of far-field ground motion excitations on building frames, which are characterized by symmetric, relatively small amplitude cycles (Sabelli et al. 2003). In the companion paper (Lanning et al. 2015), two near-fault BRB loading protocols were developed that contain deformational demands significantly greater than the AISC protocol.

This paper summarizes the results and observations from a full-scale testing program that utilized these protocols to demonstrate the ability of commercially available BRBs to sustain the demands required for implementation on long-span bridges near seismic faults. Furthermore, the implications on seismic capacity design due to large asymmetric inelastic cycles, steel core material, and strain rate effects on BRB response are presented, and recommendations are provided.

Testing Program

Specimens

A total of six full-scale BRBs were donated by CoreBrace, LLC (West Jordan, UT), one of three BRB manufacturers in the United States. The specimens were nominally 6 m in length and comprised

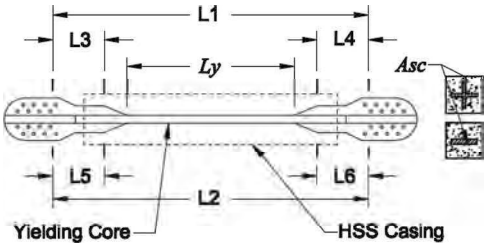

Fig. 2. Specimen dimensions and instrumentation

two sets of three geometrically identical braces. The six yielding cores were fabricated from four steel plates; cores of Specimens 1–4 were made from two ASTM A240 Type 304/304L (ASTM A240 2015) stainless steel (SS) plates, whereas those of Specimens 4 and 5 were made from two different A36 steel plates. Brace yielding core length (L_y) and cross-section area (A_{sc}) are shown in Fig. 2. According to the available literature, BRBs with SS yielding core had never been studied before. Although more expensive than A36 steel, the much more ductile SS may in some situations be more attractive for BRB bridge applications in a more corrosive environment.

Yielding core material and brace properties are provided in Tables 1 and 2. Along with material tensile tests provided by the BRB manufacturer, the authors conducted independent tensile coupon tests of the SS plates at pseudostatic and high strain rates (0.25 mm./mm./s or 25% s^{-1}). The resulting monotonic loading curves are shown in Fig. 3; the results are discussed later.

Test Setup

The specimens were tested at the Seismic Response Modification Device (SRMD) facility at the University of California, San Diego. Fig. 4 shows an installed specimen on the SRMD shake table. One end of the brace was connected to a strong wall (left side in photo), and the other was connected to a reaction block attached to the shake table. Each end of the extended core plate was connected to gusset plates with ASTM F2280 (2014) tension-controlled bolts, creating a slip-critical connection. This connection was designed to resist slip up to the brace initial yield force, and therefore, bolt slip was expected and experienced in all tests; however, no effect on the hysteretic behavior was observed. Only uniaxial deformations were imposed in this study, unlike those in the AISC protocol, which incorporate transverse motions consistent with member end rotations in a frame. Although three specimens underwent the AISC protocol, only Specimen 2 included these lateral deformations.

A redundant set of string potentiometers, labeled L1 and L6 in Fig. 2, were used on each specimen to measure the deformation along the core plate and were sampled at a frequency of up to 500 Hz for the dynamic tests. Potentiometers L1 and L2 measured the whole deformation over the core, whereas L3–L6 each measured one-half of the core deformation on either side of the Hollow Structural Section (HSS) casing. The brace forces were measured by the load cell in each of the four actuators that drive the SRMD table. Video was recorded for each test specimen, several of which are provided on the Internet (Lanning and Uang 2014).

Loading Protocols

The proof and near-fault protocols (Lanning et al. 2015) are shown in Figs. 5(a and b), with the near-fault–induced strain pulse oriented in the tension direction. Note that the timescale applies only to the dynamic versions of these protocols. The

Table 1. BRB Steel Core Material Properties

Specimen number	Steel type	Strain rate	F_{ya} (MPa)[a]	R_y[b]	F_{ua} (MPa)	R_t[b]	R_u	2-in. gauge length elongation (%)
1, 4	Stainless Type 304, Type 304/304L	PS	272	1.58	636	1.32	2.34	54
2, 3		PS	228	1.33	663	1.26	2.88	57
		25	270	1.58	609	1.26	2.26	69
5	A36	PS	285	1.15	450	1.15	1.58	40
6			282	1.14	490	1.14	1.73	33

Note: PS = pseudostatic test provided by BRB manufacturer; rate assumed to approximately 0.025% s^{-1}.
[a]Based on 2% strain offset.
[b]Assuming Type 304L specifications.

Table 2. BRB Specimen and Loading Characteristics

		Core plate				BRB			Tested protocol sequence			
Specimen number	Test order	Steel grade	Shape[a]	A_{sc} (cm^2)	L_y (m)	P_{ya} (kN)	Δ_{by} (mm)	Loading rate	1st	2nd	3rd	4th
1	1	SS	+	103	3.2	2,808	5.8	PS	Proof T	Proof C[b]	N/A	N/A
2	2					2,370	5.1	PS	Proof C	Near Fault T	AISC	N/A
3	4		–	52	3.8	1,186	5.6	D	Proof C	Near Fault C	AISC	LCF[c]
4	5					1,404	6.6	PS	Proof C	Near Fault C	AISC	N/A
5	3	A36	+	103	3.2	2,946	5.8	PS	Near Fault T	Near Fault C	N/A	N/A
6	6		–	52	3.8	1,459	6.6	D	Proof C	Near Fault C	AISC[d]	N/A

Note: PS = pseudostatic loading rate; D = dynamic loading rate; LCF = low-cycle fatigue protocol.
[a]+ and – designate cruciform and flat-plate cross section, respectively.
[b]Specimen 1 experienced a connection instability.
[c]Fracture occurred.
[d]Fracture occurred.

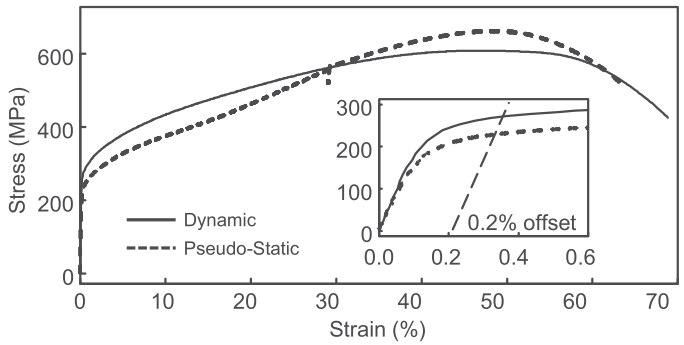

Fig. 3. ASTM A240 Type 304/304L tensile coupon tests at pseudo-static and dynamic loading rates

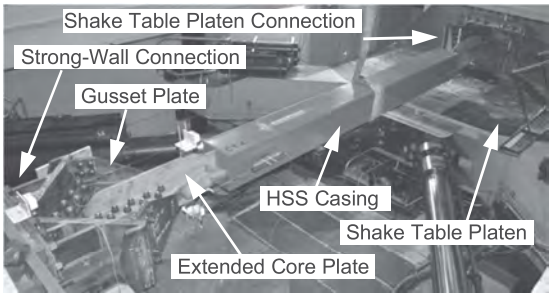

Fig. 4. Specimen setup in SRMD facility

AISC protocol is shown in Fig. 5(c). Proof and near-fault protocol tests were conducted with the peak strain pulse in both tension and compression directions, referred to as Proof T, Proof C, Near Fault T, and Near Fault C. Various combinations and sequences of these protocols were applied to the specimens to investigate the inelastic capacities of the braces and to explore any resulting sequence effects.

The dynamic versions of the near-field protocols were developed by Lanning et al. (2015), but a dynamic AISC protocol was also used in this program. Note its much smaller symmetric cycles, given by AISC 341-10 and shown in Fig. 5(c), that were established in consideration of the statistical demands of far-field ground motion on buildings with BRBFs (Sabelli et al. 2003). The current provisions of AISC 341-10 ignore the strain rate effect by not requiring BRBs to be loaded dynamically. Here, by assuming the elastic period (≈0.6 s) for a six-story BRBF, as calculated in ASCE/SEI 7-10 (ASCE 2010) and used by Sabelli et al. (2003), the maximum strain rate was estimated to be 11% s^{-1} during the maximum amplitude cycles. The timescales for the remaining sets of cycles were scaled in proportion to their relative deformation to provide smooth velocity and acceleration time histories for machine operation. These deformations were converted to yielding core strains, resulting in the dynamic AISC protocol (see Lanning et al. 2013).

The specimen test order, loading protocols used, sequence in which they were applied, and type of loading rate for each specimen are provided in Table 2. Specimens 1, 2, and 5 were tested with increasingly demanding protocols to obtain confidence in the ability of BRBs to withstand the aggressive deformation demands. After three successfully tested braces, Specimens 3, 4, and 6 were then subjected to the exact same deformations to facilitate comparisons. Specimens 3 and 6 were loaded

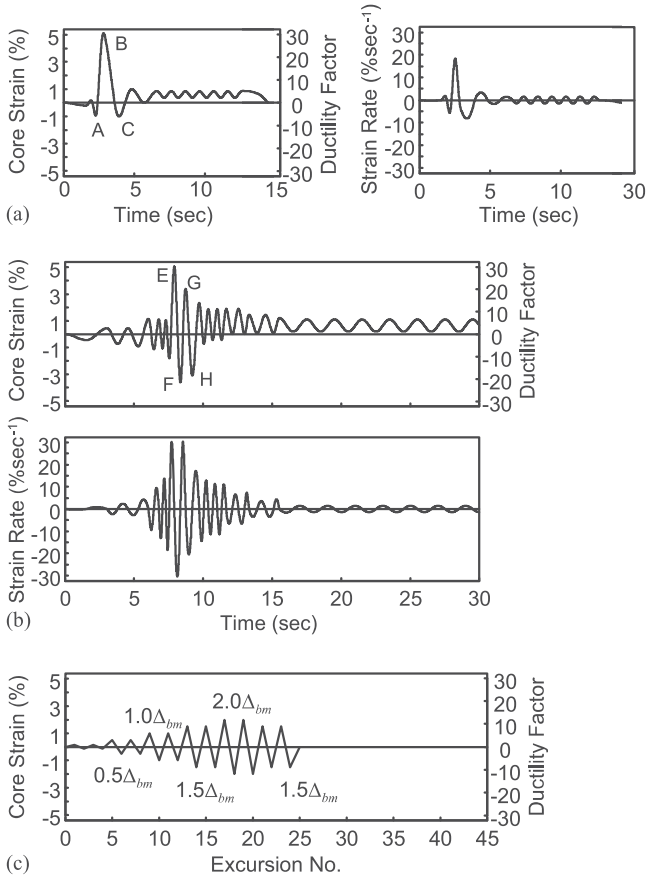

Fig. 5. BRB loading protocols: (a) proof; (b) near fault; (c) AISC (timescales apply only to dynamic tests)

dynamically with the same strain rates to readily compare the rate effects of yielding core steel type. Specimen 4 was tested pseudostatically to provide a one-to-one comparison with Specimen 3 with loading rate as the only variable.

Overall Performance

The hysteretic performance of each specimen is displayed in Fig. 6, whereas maximum brace forces and deformations are listed in Table 3. Brace deformation (Δ) is provided in terms of core strain and is calculated over the length L_y and as a ductility factor, found by normalizing Δ by the yield deformation (Δ_{by}). Maximum brace forces are shown normalized by the respective yield force (P_{ya}) calculated from the pseudostatic core plate yield stresses listed in Table 1.

As indicated in Table 2, only Specimens 3 and 6 were taken to fracture; to facilitate their removal from the testing equipment and for further examination of the steel core buckling shape, the other specimens were not taken to fracture. Each specimen withstood at minimum one loading protocol test with a BRB core strain of 5% (bolt slip occasionally led to minor deviations from target core deformation), whereas most were subjected to two near-fault loading protocol tests and a subsequent AISC protocol.

All braces performed very well, showing no signs of strength degradation before test termination or fracture. Each sustained large cumulative inelastic ductility (η) which is an indication of the accumulated sustained material damage and is commonly approximated in AISC prequalifying tests by first finding the inelastic ductility of the *i*th cycle

$$\mu_i = \frac{2|\Delta_i^+ - \Delta_i^-|}{\Delta_{by}} - 4 \tag{1}$$

where Δ_i^+ and Δ_i^- = algebraic peak positive and negative deformations; and; the elastic portion is removed by subtracting $4\Delta_{by}$. Then, the sum of the normalized deformations provides the cumulative ductility

$$\eta = \sum \mu_i \tag{2}$$

AISC 341-10 requires that η of at least 200 be achieved during the AISC protocol for prequalification. Strictly speaking, this AISC requirement does not apply to this testing program because near-field loading protocols were used, but it is evident that all BRBs (except Specimen 1, discussed later) far outperformed this requirement.

The total energy dissipated by each brace is found as the area under the force–deformation curve by

$$E_h = \int P \cdot d\Delta \tag{3}$$

where P = brace force. For cross-specimen comparison, dissipated the energy can be normalized as

$$\psi_h = \frac{E_h}{P_{ya}\Delta_{by}} \tag{4}$$

where P_{ya} = actual brace yield force calculated from the measured yield stress of the core plate (F_{ya}) (see Tables 1 and 2). The relative amounts of dissipated energy for each of the six BRBs is also shown in Table 3.

Specimen 1, which was the first specimen tested, successfully completed the Proof T test. In an attempt to apply a subsequent Proof C test, however, the specimen experienced an unexpected connection instability, as shown in Figs. 7(a and b). This failure mode has been observed in several other BRB testing programs (Tsai et al. 2008) and in predictive models presented by Takeuchi et al. (2014), among others. Gusset plates with free-edge stiffeners and new connection brackets with thicker gusset-to-bracket bolting plates were used successfully for the remaining five braces. The improved end condition is displayed in Fig. 7(c). This solution is consistent with other researchers encountering or studying this connection behavior.

Specimen 3 exhibited a slight casing bulge near one end of the restrained core. This type of deformation, which has been documented by others (e.g., Iwata 2004; Chou and Chen 2010) for BRBs with flat-plate cores, is indicative of restrained strong-axis buckling of the core within the restraining member. Note that no loss of brace resistance was experienced due to this internal buckling, even at the relatively large deformation levels of 5% compressive core strain.

Analysis of Results

Effect of Large Nonsymmetric Cycles

The conventional measurement of the imbalance between compression and tension force responses of a BRB is the compression strength adjustment factor (β) described earlier. Fig. 8(a) displays the way in which β is experimentally measured and how it is applied to a frame in design, where $\beta > 1.0$ per AISC. The value is measured as the ratio of the subsequent peak compression to tension

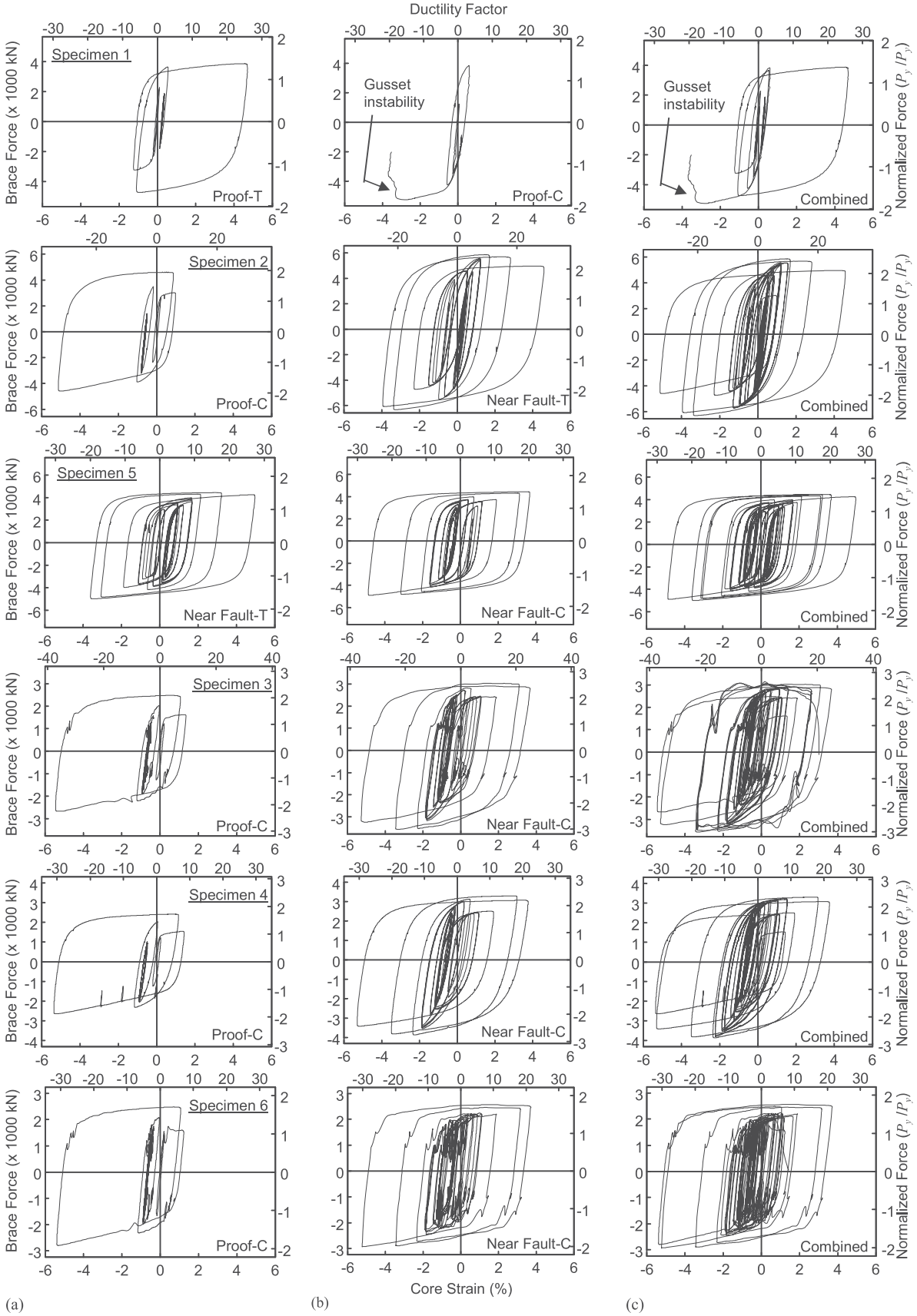

Fig. 6. Hysteretic response of test specimens: (a) first test; (b) second test; (c) all test responses combined

Table 3. Maximum Response Values

Specimen	Normalized force		Core strain		Strain rate (% s^{-1})	(P_y/P_{ya}) (×1,000 kN · m)	E_h	ψ_h
	Tension	Compression	Tension	Compression				
1	1.38	–1.87	4.72	–2.62	PS	2.2	133[a]	112[a]
2	2.47	–2.67	4.57	–5.14	PS	12.3	1,024	724
3	2.55	–3.01	3.68	–5.45	36.5	13.6	2,052	1,221
4	2.35	–2.76	3.75	–5.36	PS	10.9	1,177	820
5	1.51	–1.69	5.02	–4.83	PS	14.8	859	747
6	1.76	–2.01	3.71	–5.39	36.7	8.6	888	733

Note: PS = pseudostatic test.
[a]Specimen 1 experienced a connection instability.

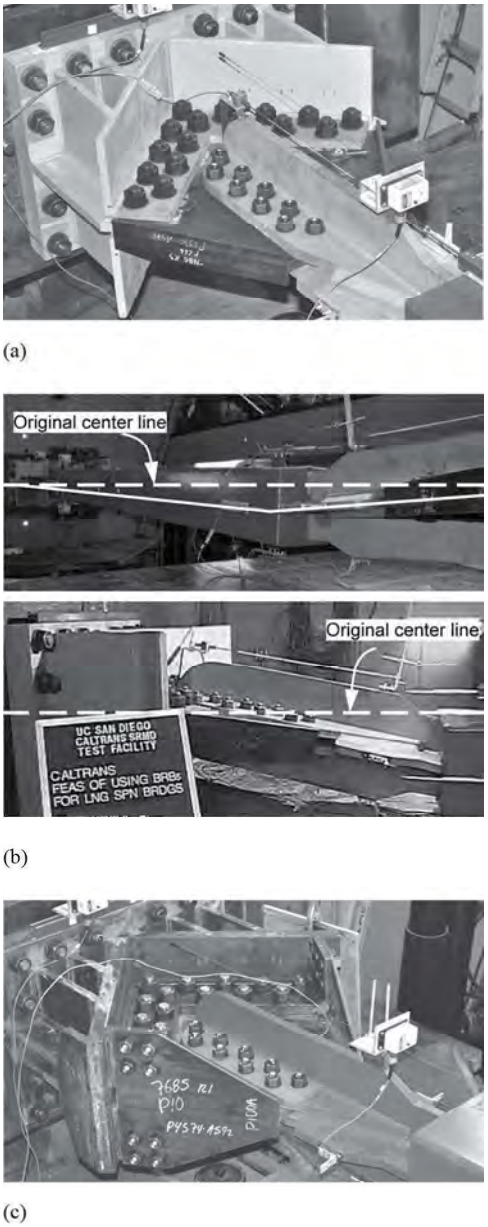

Fig. 7. Specimen end conditions: (a) Specimen 1 only; (b) gusset failure; (c) Specimens 2–6

forces, $P_{t_2}(\beta\omega P_y)$ and $T_{t_1}(\omega P_y)$, during each of the symmetric cycles of the AISC protocol applied to a single BRB. Then, for the capacity design of the horizontal member with two adjoining braces, the resultant force between the two is proportional to β. Note that, when following the current provisions, the resultant force is always applied upward because β is only taken as greater than 1.0, and the resultant is always found from the difference between $\beta\omega P_y$ and ωP_y, as indicated in Fig. 8(a), from subsequent excursions.

However, this method is not consistent with actual loading in the structure because it considers the loading sequence and brace response of a single brace, whereas there are two braces in the structure that are loaded in nominally equal but opposite sequence. The deformation time history and hysteretic behavior of two such braces, illustrated in Fig. 8(b), would provide a consistent representation of the brace forces and the ensuing resultant force between the two. Brace 1 is loaded in tension, whereas Brace 2 is simultaneously loaded in compression at time t_1 and vice versa at time t_2. Here, the unbalanced force is found at each deformation peak for each brace, with maximum tension and compression forces taken from the appropriate BRB. In Fig. 8(b), the unbalance at each time instance is shown and illustrates the case in which the resultant force is in the downward, not upward, direction, which is a scenario the current methodology ignores.

However, to facilitate the economy of prequalification testing, currently only one BRB is required to be tested for the measurement of β per the provisions of AISC 341-10. Also, given the fairly symmetric and regular hysteretic behavior of many braces tested using the symmetric cycles of the AISC protocol (e.g. Merritt et al. 2003; Tremblay et al. 2006), this inconsistent approach may still provide equal or even conservative estimates of the unbalanced forces due to the relatively small deformations of many cycles and low amounts of strain hardening exhibited by typical A36 yielding core BRBs.

On the other hand, the meaning, validity, and measurement of β are unclear when amplitudes in a cycle are not symmetric. Refer to the deformation time histories and hysteretic responses for the first three proof protocol excursions of Specimens 1 and 2 shown in Figs. 9(a and b). If β is conventionally evaluated for Specimen 1 with the strength ratio P_{t_3}/T_{t_2}, a value of 1.22 will result, but a much larger value (1.52) will result for the nominally identical brace Specimen 2 if β is calculated as the force ratio P_{t_2}/T_{t_1}. Such inconsistency is due to the unequal magnitude deformations at which the forces are measured, which violates the implied definition of β in AISC 341-10. This conventional method is not consistent with actual loading and is not well suited for nonsymmetric loading, especially when cycles contain large strain amplitude. A better definition of the unbalanced force is desirable.

Consider, again, the chevron configuration shown in Fig. 8, and assume that the nominally identical Specimens 1 and 2 represent the two braces in the frame. As shown in Fig. 9, asymmetric cycles from a near-field seismic event can result in more than one scenario

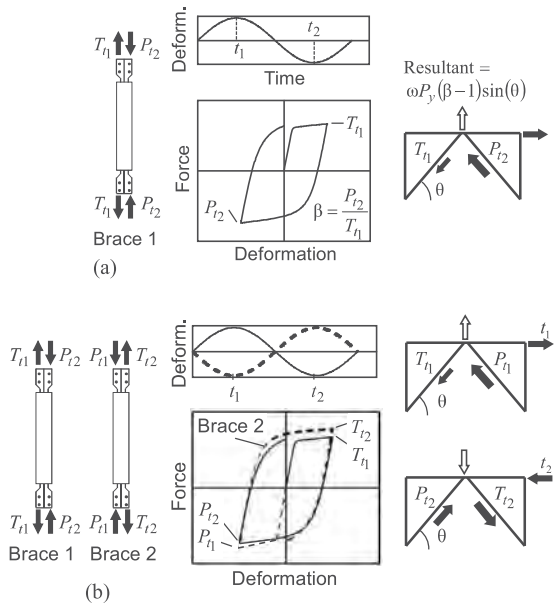

Fig. 8. Unbalanced brace forces from: (a) a single brace; (b) a set of braces

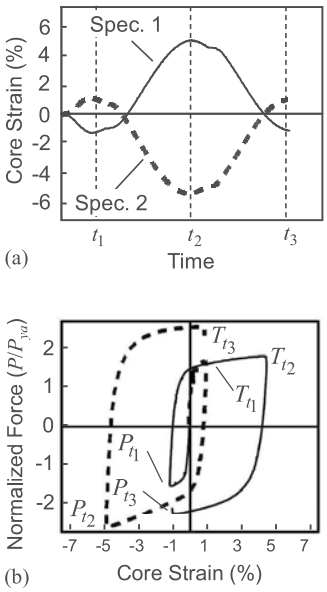

Fig. 9. Effect of large nonsymmetric cycles on BRBs: (a) deformation time histories; (b) hysteretic responses

of unbalanced forces, such as the two in Fig. 8(b), causing a resultant force in either direction perpendicular to the horizontal member. An upward resultant is experienced during loading of t_2 because $P_{t_2} > T_{t_2}$, shown in Fig. 9(b). Likewise, during loading of t_3, the resultant is in the downward direction as $T_{t_3} > P_{t_3}$. Both scenarios must be addressed in designing the horizontal member.

Because of these inadequacies of β as defined and utilized in AISC 341-10 for far-field ground motions, the unbalanced strength factor is proposed, which can be measured during near-field BRB prequalifying tests as

$$\gamma_i = \frac{|\omega_{C,i}|}{\omega_{T,i}} \tag{5}$$

where $\omega_{C,i}$ and $\omega_{T,i}$ = compression and tension overstrength factors, respectively, for the ith excursion measured from a pair of nominally identical braces subjected to equal and opposite loading protocols. The compression and tension factors are numerically equal to the peak force normalized by P_{ya}. Measuring the unbalance in this way is consistent with the interaction between adjacent, or opposing, braces of many possible BRB configurations. Multiple cases of unbalanced brace forces can be identified, unlike in the current provisions, by recording a maximum and a minimum value of γ. Additionally, the maximum values of ω_C and ω_T in the two tests provide the maximum individual brace compression and tensile forces, respectively, under two loading sequences as opposed to only one required by the current testing convention. The maximum ω_C can be utilized within the modified Thornton method conventionally for the design of the brace gusset plates, whereas ω_T can provide the maximum tension force in checking the Whitmore section of the gusset plate for yielding and rupture.

The values of ω_C, ω_T, and γ corresponding to the tests conducted on Specimens 1 and 2, shown in Fig. 9, are provided in Table 4. At t_2, with nearly 5% core strain, γ is shown to be 1.39, indicating that the brace in compression exhibits a larger magnitude force than the brace in tension. Conversely, brace forces at t_1 and t_3 produce γ values less than 1.0, meaning tension forces are larger than compression forces. Because only one pair of specimens was subjected to equal and opposite protocol, the full effects and range of acceptable γ values are yet unknown. Limiting the unbalance in either case to 30% (i.e., limiting β to 1.3 in AISC 341-10) seems reasonable; however, exception may be required for large core strains of the near-fault pulse excursions because the unbalance was found to be almost 1.40 at 5% core strain. Testing more BRB designs will provide more information to set limits for γ in both tension and compression unbalance scenarios. However, before more test data are available, reasonable limits for γ are suggested to be held to a minimum of 0.70 and a maximum of 1.40.

To provide meaningful strain-hardening factors for near-field applications, it is suggested that a pair of nominally identical specimens, not one specimen, be tested. To further demonstrate the problem associated with the latter, consider the first and second tests applied to Specimen 2, shown in Fig. 10. These contain subsequent 5% core strain excursions from which a γ value can be attempted. Fig. 10(b) shows the two branches of the hysteretic curve for these excursions. Per Eq. (5), the value of γ is then found to be 0.91 (–1.92/2.1) for the subsequent, nearly 5% core strains. Clearly, the sequence of loading has a dramatic effect on γ and hence the considered unbalanced loading cases. Had the excursions occurred in the reverse order (tension before compression), the value of γ would likely be very different. This and the reasons listed earlier suggest that proper BRB testing should include two nominally identical braces subjected to equal yet opposite loading protocols from which the unbalanced force can be obtained in a consistent manner.

Measuring ω_C, ω_T, and γ in the proposed manner permits the proper design of chevron-style frames, such as BRBFs in buildings and in the bridge applications studied by Usami et al. (2005) and Kanaji et al. (2005). Knowledge of the multiple possible cases of unbalanced BRB loading given by γ, and not by β, is particularly important in designing the reinforcing steel for reinforced concrete beams, slabs, or abutment structures for BRB bridge applications, such as those used in ductile end diaphragms investigated by Celik and Bruneau (2009), shown in Fig. 11(a). Other possible BRB arrangements, such as those of the viscous dampers on the Rio-Antirion Bridge (Infanti et al. 2004), similar to that shown in Fig. 11(b), could affect the structure design where unbalanced forces

Table 4. Measured Unbalanced Forces (η) from Equal and Opposite Tests (Specimens 1 and 2)

	Peak core strain			Normalized peak forces		
Excursion number	Time	Specimen	%	ω_T	ω_C	γ
1	t_1	1	–1.0		–1.15	0.90
		2	1.0	1.28		
2	t_2	2	–4.7		–1.92	1.39
		1	4.7	1.38		
3	t_3	1	–0.9		–1.68	0.86
		2	0.9	1.95		
γ_{max}						1.39
γ_{min}						0.86

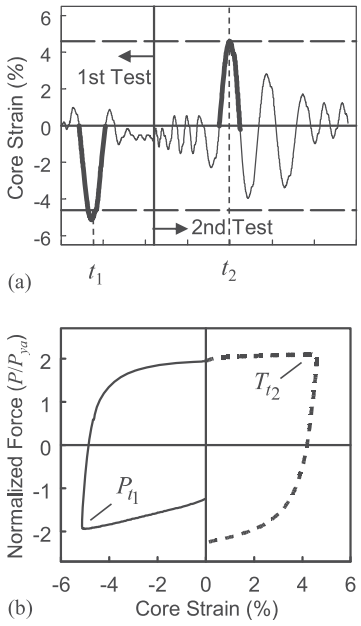

Fig. 10. Subsequent large excursions of Specimen 2: (a) deformation time history; (b) hysteretic response

cause torsion on the bridge span. For common bracing systems in which BRBs do not oppose each other, such as in diagonal bracing configurations with parallel braces in each bay, testing as proposed also provides the maximum overstrength achieved under two different loading sequences, unlike in the current AISC provisions, for use in capacity-based design of the frame and connections.

Effect of Yielding Core Steel Type

The geometrically identical Specimens 3 (SS) and 6 (A36) were subjected to the same dynamic loading protocols with equal strain magnitudes, which were tested to fracture. The superior ductility capacity and energy dissipation capability of SS is displayed in Specimen 3, which sustained an η of 1.67 and ψ_h 2.31 times greater than Specimen 6, as summarized in Table 3. Extrapolating only from these two BRBs, Specimen 5 (A36) appears to have been very close to fracture, whereas Specimens 1, 2, and 4 (all SS) were likely capable of sustaining one additional protocol at minimum. Furthermore, tensile coupon tests of the two materials in this research (Table 1 and Fig. 3) show, on average, the elongation at failure to be 1.56 (0.56/0.36) times greater for the SS over A36.

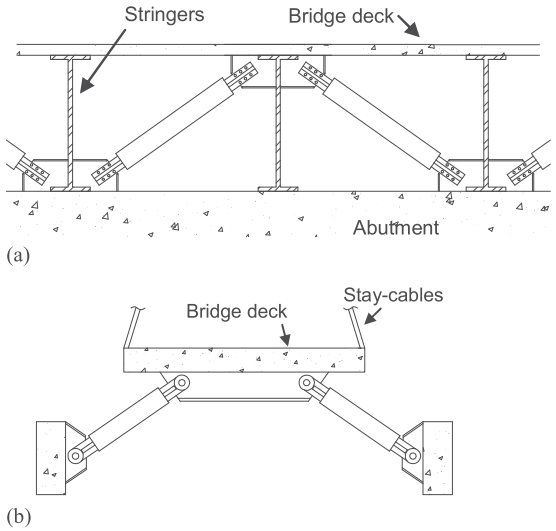

Fig. 11. (a) BRBs in bidirectional resistant ductile end diaphragms; (b) BRBs in the configuration of existing viscous dampers on the Rio-Antirion Bridge

Compared with that of A36 steel, the desirable corrosion resistance and ductility of SS, Type 304/304L among other grades, is accompanied by significantly different strain-hardening behavior. An indicating factor of the hardening potential of a steel material is the $R_u(F_{ua}/F_{ya})$ value obtained from tensile coupon tests. The material test results in Table 1 show the average SS-to-A36 R_u ratio to be 1.51 (assuming pseudostatic loading), indicating that SS has much more potential for strain hardening than A36. This is reflected by the very different cyclic strain hardening (CSH) behavior of the two materials, which can be compared in terms of two common rules known as kinematic and isotropic hardening, or the translation and dilation of the material yield surface, respectively. SS is known to exhibit significant isotropic hardening, as shown by Paul et al. (2010), whereas cyclic tests on A36 steel coupons by Kaufmann et al. (2001) showed its hardening to be mostly kinematic in nature. Also, Nip et al. (2010) performed extremely-low-cycle fatigue tests on carbon steel and SS coupons, which also clearly showed these CSH differences. The CSH behaviors are clearly displayed by the BRB tests performed in this research.

Significant cycles from the BRB tests are shown in Fig. 12 for clarity, where the marked events correspond to those shown in Figs. 5(a and b). As shown in Fig. 13(a), the SS-to-A36 normalized peak force ratio averaged 1.19 for Events A–C and continued to increase throughout the second test, averaging 1.45 and reaching a maximum of 1.52. These hysteretic loops revealed the isotropic CSH behavior of SS and the kinematic hardening of A36 by inspecting Points B, D, and F. At Event D, the deformation was nearly equal to that of Event B, yet the peak force for SS increased by 1.21 (2.73/2.25), whereas that of the A36 brace was only 1.05 (2.01/1.91) times greater than at Event B. Furthermore, the deformation level of Event F was attained by each brace twice, occurring first along the curve leading to Event D. Comparing the normalized peak forces upon returning to deformation of Event F, the SS force increased by 1.18 (3.01/2.57), whereas A36 increased by only 1.05 (1.98/1.88). This clearly demonstrates the significantly different isotropic CSH behavior of the two materials. Note that, despite the considerable deformation and η differences at all three points, the A36 brace exhibited essentially the same normalized peak forces at both Events D and F ($\approx$2.0).

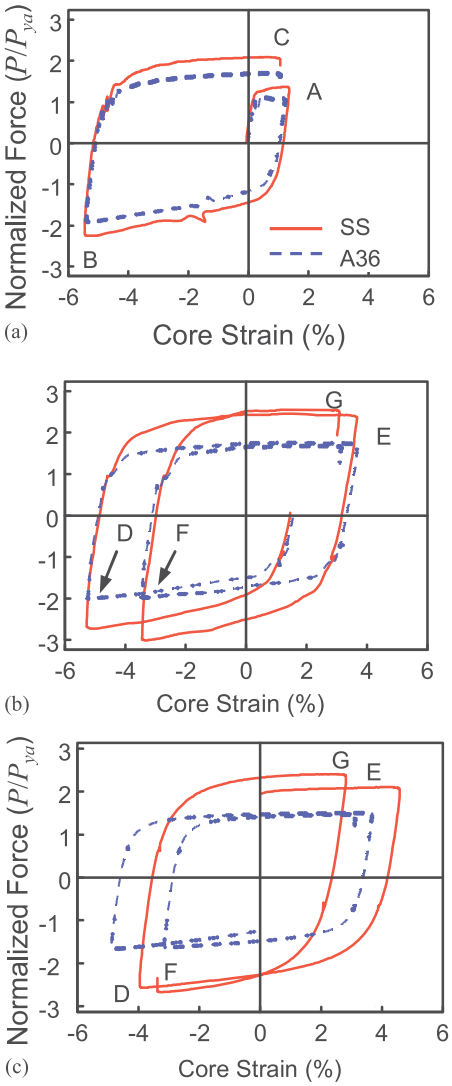

Fig. 12. Effects of yielding core material: (a) first test for Specimens 3 and 6, Proof C; (b) second test for Specimens 3 and 6, Near Fault C; (c) second tests for Specimens 2 and 5

Effect of Strain Rate

Mild structural steels such as A36 are generally assumed as rate-independent because the yield stresses are typically only approximately 7% higher under seismic loading rates (Di Sarno et al. 2002). SS is recognized as more strain rate–dependent, as summarized by Nordberg (2004) with flow stresses (stress required to continue deforming plastically) at both 0.2 and 2% strains approximately 1.28 times greater due to an increase in strain rate from 0.1 to 100% s^{-1}. Despite the general dismissal of the strain rate effect for structural steels due to the relatively low strain rates expected in structures under earthquake loading on the order of 10% s^{-1} (Shing et al. 1988), several researchers have recognized that bracing members can experience high rates at sites of local inelastic behaviors, such as plastic hinges at mid-length in buckled braces, during large seismic loading. Carden et al. (2004) performed dynamic tests on short BRBs, within ductile end frames of bridge spans, under a constant frequency of 2 Hz, resulting in a maximum core strain rate of 13.8% s^{-1}. Tremblay et al. (2006) subjected BRBs to dynamic loading, leading to a maximum rate of 25% s^{-1}. These cases were reported to

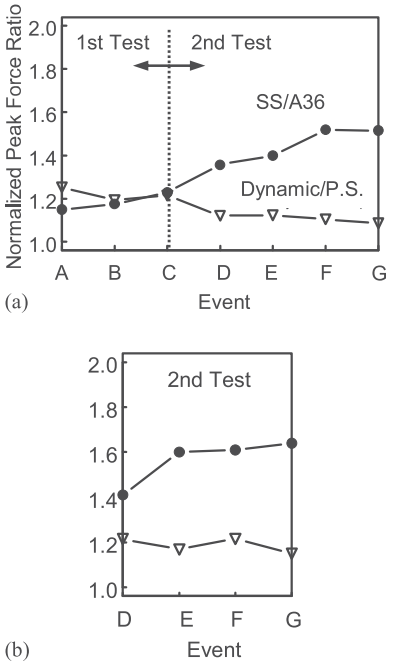

Fig. 13. Relative normalized peak force values as a ratio: (a) Specimens 3–6 and 3–4; (b) Specimens 2–5 and 5–6 (Note: P.S. = pseudo-static)

have increased BRB hysteretic responses by 15 and 5%, respectively, compared with similar pseudostatically loaded braces. During the protocol development by the authors (Lanning et al. 2015), simulated BRB yielding core strain rates had a mean (18.9% s^{-1}) plus one standard deviation (11.2% s^{-1}) of 30% s^{-1}, with a maximum of 50% s^{-1}. The former is represented in the dynamic near-fault protocol, shown in Fig. 5(b).

The nominally identical SS Specimens 3 and 4 were subjected to the same protocols, but with dynamic and pseudostatic loading rates, respectively. Significant cycles are shown in Figs. 14(a and b), with brace forces normalized by P_{ya} assuming the BRB manufacturer-provided coupon test results conducted at a pseudostatic loading rate (Table 1). In Fig. 13(a), Events A–C of Specimens 3 and 4 show that initially, on average, the dynamic-to-static normalized peak force ratio averaged 1.22. Throughout the second test, despite strain rates and η being much larger, the peak force ratio decreased to an average of 1.11 (Events D–G). Over both tests, dynamic-to-pseudostatic normalized forces were approximately 1.16 larger. This is consistent with the dynamic effect on BRB found by the researchers as mentioned earlier. The excursions of the second test reflect the SS strain rate behavior summarized by Di Sarno et al. (2002), as the larger strain excursions exhibit less rate effect. Also in agreement with those findings is the reduction of R_u found in the dynamic coupon test presented in Table 1 and Fig. 3. This indicates a decreased spread of plasticity along the coupon at a higher rate, and therefore the increase in force due to high rate is expected to decrease or stabilize with increasing η under high strain rate loading conditions.

Finally, similar ratios were found from the significant cycles of the second tests performed on Specimens 5 (pseudostatic) and 6 (dynamic) of A36 steel, shown in Fig. 14(c). Similarly, the dynamic normalized forces averaged 17% greater than those from the pseudostatic tests, shown in Fig. 13(b). Despite their differing first test protocols, the primarily kinematic CSH of A36 permits the direct comparison of these two specimens (i.e., the material is essentially strain history–independent).

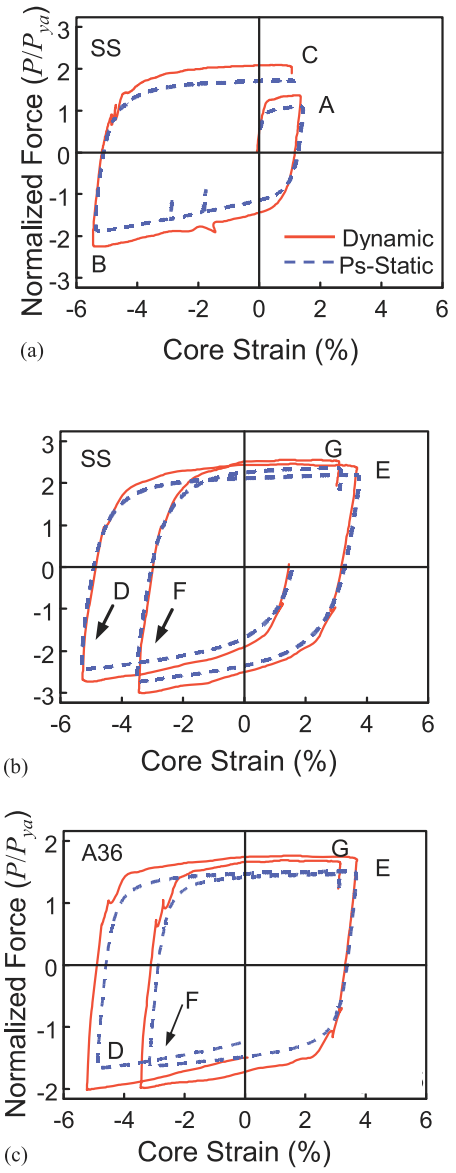

Fig. 14. Effect of strain rate: (a) first test for SS Specimens 3 and 4, Proof C; (b) second test for SS Specimens 3 and 4, Near Fault C; (c) second tests for A36 Specimens 5 and 6 (Note: Ps-Static = Pseudo-Static)

Summary

In the companion paper (Lanning et al. 2015), replacing viscous dampers with BRBs on the long-span Vincent Thomas Bridge was shown to be both feasible and beneficial. Loading protocols, statistically representative of the expected BRB deformation demands, were developed for qualifying BRBs for use on many existing near-fault long-span bridges. In this paper, these protocols were utilized in the full-scale testing of six commercially available BRBs, and their ability to sustain the large strain (5%) demands under both pseudostatic and fully dynamic loading rates of more than 30% s^{-1} was demonstrated. Furthermore, the braces were shown to be capable of sustaining consecutive protocols resulting in large amounts of cumulative ductility (η) and hysteretic energy (E_h). For example, those applied to Specimen 5 considered together are not realistic, but show the significant reserve deformation capacity even after a major near-field ground excitation. This and the other specimen results support the use of BRBs as highly ductile metallic dampers beyond their current U.S. role as solely ductile structural fuses, given their capabilities of providing stable hysteretic response over numerous large seismic events representing subsequent rare earthquake demands.

Large asymmetric inelastic cycles were shown to result in multiple possible cases of compression-to-tension unbalanced BRB forces. This demands attention be paid to the intended BRB arrangement and to the loading sequence used in testing, where the unbalanced force factor (γ) can be measured from two nominally identical braces subjected to equal yet opposite protocols. Multiple unbalanced brace force scenarios can thereby be identified for use in the capacity design of the surrounding structure.

SS A240 Type 304/304L BRBs were shown to be very resilient in inelastic deformation and energy dissipation capabilities; however, the significant cyclic strain-hardening behavior of SS must be taken into consideration in designing the adjoining members. Similarly, high strain rates have been shown to occur in BRBs on long-span bridges (Lanning et al. 2015), and the resulting experimental brace forces were observed to be, on average, 17% larger than those obtained from pseudostatic testing.

Acknowledgments

Funding for this research was provided by the California Department of Transportation under Contract No. 65A0358, with Dr. Charly Sikorsky as the project manager. The authors thank CoreBrace, LLC, for donating the specimens.

Notation

The following symbols are used in this paper:

A_{sc} = yielding core area;
E_h = hysteretic energy;
F_{ua} = measured steel tensile strength;
F_{ya} = measured steel yield stress;
L_y = yielding core length;
P_{ya} = brace yield force based on F_{ya};
P_{yn} = nominal brace yield force;
R_t = material overstrength factor, $F_{ua}/F_{u,\text{nominal}}$;
R_u = material hardening factor, F_{ua}/F_{ya};
R_y = material overstrength factor, $F_{ya}/F_{y,\text{nominal}}$;
β = compression strength adjustment factor defined in AISC 341-10;
γ = BRB unbalanced strength factor;
Δ = BRB deformation;
Δ_{bm} = design story drift;
Δ_{by} = BRB yield deformation;
η = cumulative ductility;
ψ_h = normalized hysteretic energy;
ω = tension strength adjustment factor defined in AISC 341-10;
ω_C = compression overstrength factor;
ω_T = tension overstrength factor;
$\omega_{C,i}$ = compressive cyclic overstrength factor for ith excursion; and
$\omega_{T,i}$ = tensile cyclic overstrength factor for ith excursion.

References

AISC. (2005). "Seismic provisions for structural steel buildings." *AISC 341-05*, Chicago.
AISC. (2010). "Seismic provisions for structural steel buildings." *AISC 341-10*, Chicago.

ASCE. (2010). "Minimum design loads for buildings and other structures." *ASCE 7-10*, Reston, VA.

ASTM. (2014). "Standard specification for 'twist off' type tension control structural bolt/nut/washer assemblies, steel, heat treated, 150 ksi minimum tensile strength." *F2280*, West Conshohocken, PA.

ASTM. (2015). "Standard specification for chromium and chromium-nickel stainless steel plate, sheet, and strip for pressure vessels and for general applications." *A240*, West Conshohocken, PA.

Benzoni, G., Amaddeo, C., DiCesare, A., and Palermo, G. (2008). "A damage identification procedure for bridge structures with energy dissipation devices." *Rep. No. SRMD-2007/08*, Dept. of Structural Engineering, Univ. of California, San Diego, La Jolla, CA.

Bruneau, M., Uang, C. M., and Whittaker, A. (2011). *Ductile design of steel structures*, McGraw-Hill, New York.

Carden, L., Itani, A., Buckle, I., and Aiken, I. (2004). "Buckling restrained braces for ductile end cross frames in steel plate girder bridges." *Proc., 13th World Conf. on Earthquake Eng.,* Paper No. 503, Vancouver, BC, Canada.

Celik, O. C., and Bruneau, M. (2009). "Seismic behavior of bidirectional-resistant ductile end diaphragms with buckling restrained braces in straight steel bridges." *Eng. Struct.*, 31(2), 380–393.

Chou, C.-C., and Chen, S.-Y. (2010). "Subassemblage tests and finite element analyses of sandwiched buckling-restrained braces." *Eng. Struct.*, 32(8), 2108–2121.

Di Sarno, L., Elnashai, A. S., and Nethercot, D. A. (2002). "Comparison between seismic response characteristics of carbon steel and stainless steel." *Proc., 12th European Conf. on Earthquake Eng.*, Paper No. 765, London.

Infanti, S., Papanikolas, P., Benzoni, G., and Castellano, M.G. (2004). "Rion-Antirion Bridge: Design and full-scale testing of the seismic protection devices." *Proc., 13th World Conf. on Earthquake Eng.,* Paper No. 2174, Vancouver, BC, Canada.

Iwata, M. (2004). "Applications-design of buckling restrained braces in Japan." *Proc., 13th World Conf. on Earthquake Eng.*, Paper No. 3208, Vancouver, BC, Canada.

Kanaji, H., Kitazawa, M., and Suzuki, N. (2005). "Seismic retrofit strategy using damage control design concept and the response reduction effect for a long-span truss bridge." *Proc., 19th U.S.-Japan Bridge Workshop*, Tsukuba, Japan.

Kaufmann, E. J., Metrovich, B. R., and Pense, A. W. (2001). "Characterization of cyclic inelastic strain behavior on properties of A572 Gr. 50 and A913 Gr. 50 rolled sections." *ATLSS Rep. No. 01-13*, Lehigh Univ., Bethlehem, PA.

Lanning, J., Benzoni, G., and Uang, C.-M. (2013). "The feasibility of using buckling-restrained braces for long-span bridges: Near-fault loading protocols and full-scale testing." *Rep. No. SSRP 13/17*, Dept. of Structural Engineering, Univ. of California, San Diego, La Jolla, CA.

Lanning, J., Benzoni, G., and Uang, C.-M. (2015). "Using buckling-restrained braces on long-span bridges. II: Feasibility and development of a near-fault loading protocol." *J. Bridge Eng.*, 10.1061/(ASCE)BE.1943-5592.0000804.

Lanning, J., and Uang, C.-M. (2014). "Full-scale BRB testing: Dynamic near-fault protocols." ⟨https://www.youtube.com/watch?v=zMR_uFTriHY⟩ (July. 10, 2014).

Merritt, S., Uang, C. M., and Benzoni, G. (2003) "Subassemblage testing of corebrace buckling-restrained braces." *Rep. No. TR-03/01,* Dept. of Structural Engineering, Univ. of California, San Diego, La Jolla, CA.

Moffatt and Nichol Engineers (1996). "Toll road seismic retrofit project Vincent Thomas Bridge, strategy report." *Rep. to Caltrans* California Department of Transportation, Sacramento, CA.

Nip, K. H., Gardner, L., Davies, C. M., and Elghazouli, A. Y. (2010). "Extremely low cycle fatigue tests on structural carbon steel and stainless steel." *J. Constr. Steel Res.*, 66(1), 96–110.

Nordberg, H. (2004) "Note on the sensitivity of SSs to strain rate." *Research Rep. No. 04.0-1*, AvestaPolarit Research Foundation, Sheffield Hallam Univ., International Stainless Steel Forum, Brussels, Belgium.

Paul, S. K., Sivaprasad, S., Dhar, S., and Tarafder, S. (2010). "Cyclic plastic deformation and cyclic hardening/softening behavior in 304LN stainless steel." *Theor. App. Fract. Mech.*, 54(1), 63–70.

Pollino, M., and Bruneau, M. (2007). "Seismic retrofit of bridge steel truss piers using a controlled rocking approach." *J. Bridge Eng.*, 10.1061/(ASCE)1084-0702(2007)12:5(600), 600–610.

Reno, M., and Pohll, M. (2010). "Seismic retrofit of California's Auburn-Foresthill Bridge." *Transportation Research Record*, 2201, 83–94.

Sabelli, R., Mahin, S., and Chang, C. (2003). "Seismic demands on steel braced frame buildings with buckling-restrained braces." *Eng. Struct.*, 25(5), 655–666.

Shing, P. S., and Mahin, S. (1988). "Rate-of-loading effects on pseudodynamic tests.." *J. Struct. Eng.*, 10.1061/(ASCE)0733-9445(1988)114:11(2403), 2403–2420.

Takeuchi, T., Ozaki, H., Matsui, R., and Sutcu, F. (2014). "Out-of-plane stability of buckling-restrained braces including moment transfer capacity." *Earthquake Eng. Struct. Dyn.*, 43(6), 851–869.

Tremblay, R., Bolduc, P., Neville, R., and DeVall., R. (2006). "Seismic testing and performance of buckling-restrained bracing systems." *Can. J. Civil Eng.*, 33(2), 183–198.

Tsai, K. C., et al. (2008). "Pseudo-dynamic tests of a full-scale CFT/BRB frame—Part I: Specimen design and analysis." *Earthquake Eng Struct. Dyn.* 37, 1081–1098.

Uang, C.-M., Nakashima, M., and Tsai, K.-C. (2004). "Research and application of buckling-restrained braced frames." *Int. J. Steel Struct.*, 4(4), 301–313.

Usami, T., Lu, Z., and Ge, H. (2005). "A seismic upgrading method for steel arch bridges using buckling-restrained braces." *Earthquake Eng. Struct. Dyn.*, 34(4–5), 471–496.